Characterizing UshA Cleavage Activity in *Shewanella oneidensis*

A THESIS
SUBMITTED TO THE FACULTY OF THE
UNIVERSITY OF MINNESOTA BY

Maya Restivo Burroughs

IN PARTIAL FULFILLMENT OF THE REQUIREMENTS
FOR THE DEGREE OF
MASTER OF SCIENCE

Dr. Jeffery A. Gralnick

August 2019

ACKNOWLEDGEMENTS

I would like to thank my advisor, committee, and lab mates for all of their support and input. I would also like to thank all of my wonderful friends and family, especially Asra, Asad, Diana, and Margaret.

TABLE OF CONTENTS

LIST OF TABLES

LIST OF FIGURES

CHAPTER 1
INTRODUCTION

Unprecedented climate change threatens the sustainability of natural ecosystems, global food security, and human health. The current global economy relies heavily on fossil fuels for energy production and manufacturing, releasing more carbon into the atmosphere, and worsening climate change. To slow the catastrophic effects of climate change, we need new processes for manufacturing and energy production. Biotechnological approaches present an attractive alternative. Biotechnological processes use whole "organisms, cellular extracts, or enzymes" as the basis of their production strategy and have been implemented in industries from agriculture to pharmaceuticals to bulk chemical manufacturing (Murphy 2011). Compared to traditional chemical processes, biotechnological processes often require fewer solvents and heavy metal catalysts, reducing their overall environmental impact. Most importantly, for the impending climate crisis, these approaches often use renewable feedstocks, rather than fossil fuel inputs (Murphy 2011). Thanks to the remarkable biodiversity on our planet, many organisms have evolved synthesis pathways and enzymes that produce economically-relevant outputs. These organisms can be harnessed to address pollution problems and design new production platforms with much smaller carbon footprints.

One such organism is *Shewanella oneidensis* MR-1. *S. oneidensis* MR-1 is a Gammaproteobacteria capable of respiring extracellular substrates through extracellular electron transport (EET) (Hau and Gralnick, 2007). *Shewanella* species are commonly found in aquatic environments and sediments, where oxygen availability varies (Hau and Gralnick, 2007). When oxygen is limited in these environments, *S. oneidensis* MR-1 can use over twenty electron acceptors besides oxygen for respiration, including fumarate, trimethyl amine (TMAO), dimethyl sulfoxide (DMSO), sulfite, thiosulfate, and elemental sulfur (Breuer *et al.,* 2014 Hau and Gralnick). *Shewanella* can also respire extracellular metals, including oxidized iron, manganese, chromium, and uranium (Breuer *et al.,* 2014, Hau and Gralnick, 2007). *Shewanella's* diverse respiratory ability could be applied to bioremediation and bioenergy projects.

When *Shewanella* deposits electrons onto an extracellular metal, the oxidation state of the metal changes, which alters the metal's physical properties (Breuer *et al.,* 2014). The change in physical properties could then be leveraged for environmental remediation efforts. Reduction of toxic metals arsenic and chromium, for example, makes them less soluble, causing them to precipitate (Breuer *et al.,* 2014, Hau and Gralnick, 2007). Precipitated oxides of toxic metals

could then be more easily removed from drinking water sources using microbial remediation strategies. Reduction also reduces solubility of radioactive elements such as uranium and ^{60}cobalt, which could aid in containment efforts (Hau and Gralnick, 2007). Other elements become more mobile in the environment when used as a terminal electron acceptor by *Shewanella.* For example, extracellular electron transport to insoluble iron oxides can help make the iron bioavailable to other organisms, allowing it to cycle through the environment (Kotloski *et al.*, 2013).

The ability of *Shewanella* to perform EET allows them to produce electrical current, when grown on an electrode. Thus, scientists have explored growing *Shewanella* in microbial fuel cells, as a means of alternative energy production (Kotloski *et al.*, 2013, Hau and Gralnick, 2007). *Shewanella* generates a current density of approximately 1W/m^2 (Zou *et al.*, 2019). While this rate of electricity generation is similar to other current-producing bacteria, *Shewanella* grows well in the lab, and has modern genetic tools established (Hau and Gralnick, 2007, Zou *et al.*, 2019, Corts *et al.*, 2019). *Shewanella* also has a faster generation time and less sensitivity to oxygen compared to other dissimilatory metal reducing bacteria (Hau and Gralnick, 2007). However, the rate of current production produced by *Shewanella* fuel cells is not currently competitive with traditional methods of energy production (Zou *et al.*, 2019). In order to increase the rate of current production, genetic engineering of *Shewanella* would likely be required, along with improvements to fuel cell design.

Newer ideas for *Shewanella* also include applying the organism for biosensing and microbial electrosynthesis (Zou *et al.*, 2019). Because *Shewanella* transfers electrons as a physiological response to its living conditions, *Shewanella* could act as an interface between living systems and computational systems. Changes in current production by *Shewanella* could indicate factors such as oxygen demand and media toxicity. Zou and colleagues propose that genetically engineered *Shewanella* coupled with an electrode could be designed to detect specific toxins, such as arsenic (Zou *et al.*, 2019). *S. oneidensis* could also be used for microbial electrosynthesis. Instead of transferring electrons to an electrode, *Shewanella* can also receive electrons. *Shewanella* can then use these electrons to power anabolic pathways for the production of desired chemical products. For example, *Shewanella* engineered with heterologous synthesis pathways produced isobutanol and formic acid in electrosynthesis systems (Zou *et al.*, 2019).

Biotechnological applications for *Shewanella* center on its ability to perform extracellular electron transport (Hau and Gralnick, 2007, Zou *et al.*, 2019). EET in *Shewanella* requires electrons generated from catabolic processes in the cytosol be passed through the periplasm to the

electron acceptor outside of the cell (Brutinel and Gralnick, 2011). To traverse the spatial separation between the electron donor and receptor, *S. oneidensis* passes electrons through a set of cytochromes to directly transfer electrons to extracellular substrates. *S. oneidensis* also deposits electrons on flavin molecules to shuttle electrons to the terminal electron acceptor (Brutinel and Gralnick, 2011). While many of the proteins involved in both of these pathways have been identified, questions remain about electron transfer through cytochromes and interactions between cytochromes and electron shuttles (Gralnick, 2012). All of the biotechnological applications for *Shewanella* discussed previously likely require specific pathway engineering to tailor *Shewanella's* behavior to the specific application (Zou *et al.*, 2019). To rationally design *S. oneidensis*-based systems, we need to fully understand the specifics on the functioning of both the direct and indirect electron transport pathways and how they interact.

In the direct EET pathway, shown in Figure 1, electrons are passed through a number of cytochromes, which allow for the electrons' passage across the periplasm (Gralnick 2012, Breuer *et al.*, 2014, Coursolle *et al.*, 2010). First, electrons generated from the breakdown of carbon sources in the cytoplasm are deposited onto menaquinone electron carriers in the inner membrane (Breuer *et al.*, 2014). These electrons are then passed to multi-heme cytochrome, CymA. CymA sits in the inner membrane and acts as a branch point, transferring electrons to proteins that reduce intracellular electron acceptors and to proteins that bridge the gap between CymA and outer membrane cytochromes (Gralnick 2012, Breuer *et al.*, 2014). At least two periplasmic cytochromes are known to fulfill the later role, FccA and CctA (Breuer *et al.*, 2014).

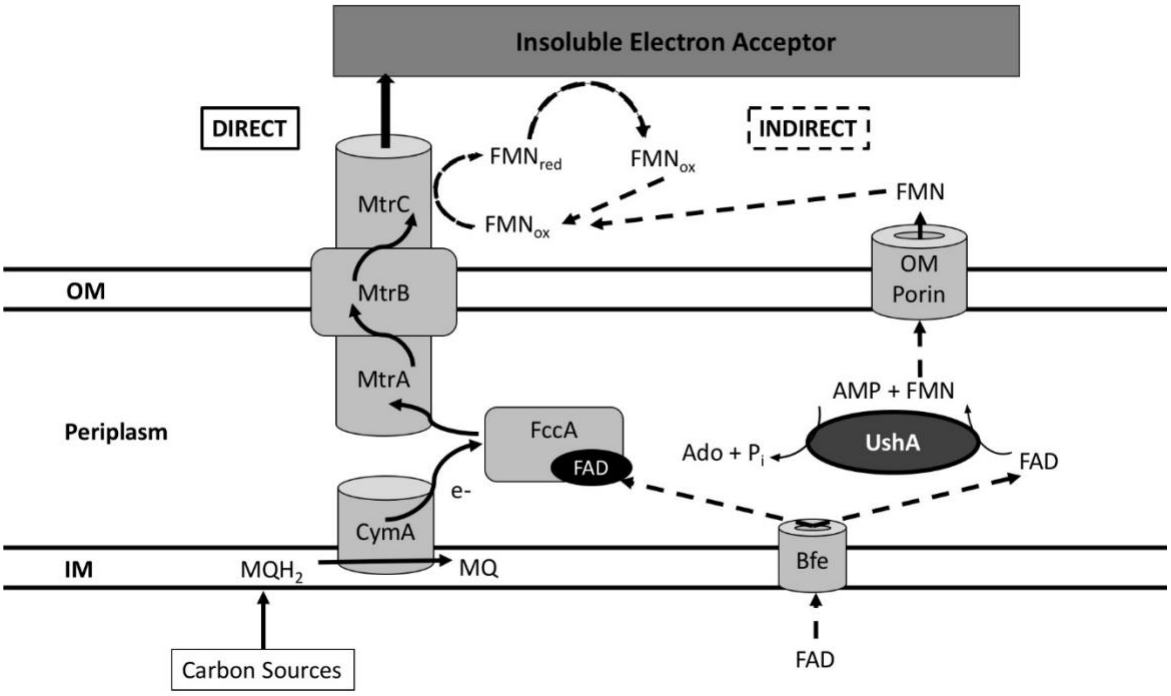

Figure 1: *S. oneidensis* MR-1 periplasm and proteins involved in EET. Solid, bold arrows show the direct pathway by which electrons from oxidation of carbon sources in the periplasm are transferred through cytochromes in the periplasm to the terminal electron acceptor. Dashed, bold arrows show the indirect pathway: FAD is exported into the periplasm, cleaved into AMP and FMN, which is then exported from the cell. FMN then acts as an electron shuttle.

Upon accepting electrons from CymA, FccA and CctA transfer them to cytochrome complexes that span the outer membrane and contact the terminal electron acceptor (Breuer *et al.*, 2014). FccA in particular is highly abundant in the periplasm and is thought to temporarily store electrons in the absence of a terminal electron acceptor (Scheutz *et al.*, 2009). When an extracellular electron acceptor is present, the MtrCAB or MtrDEF complexes make the final electron transfer through direct contact with the acceptor. MtrCAB and MtrDEF are two complexes with overlapping function that are comprised of two decaheme cytochromes connected by a membrane spanning domain (Gralnick 2012, Brutinel and Gralnick, 2011). MtrA and MtrD face into the periplasm, where they accept electrons from FccA and CctA, while MtrC and MtrF are extracellular (Gralnick 2012). MtrB and MtrE are beta-barrel porins that connect their respective intracellular and extracellular cytochromes, allowing for electron transfer through the outer membrane (Breuer *et al.*, 2014). MtrC has a putative hematite-binding domain near the heme thought to contact external electron acceptor and is involved in the reduction of iron citrate,

iron oxide, manganese oxide, and anodes (Breuer *et al.*, 2104, Bucking *et al.*, 2010). MtrF has also been shown to reduce iron citrate and manganese oxide *in vivo* (Bucking *et al.*, 2010).

In addition to direct electron transfer, *S. oneidensis* transports electrons indirectly through the use of flavin electron shuttles. Early experiments showed that *S. oneidensis* was able to reduce electron acceptors from which it was physically separated. These experiments provided strong evidence for the role of a soluble mediator in EET (Brutinel *et al.*, 2010). In one such experiment, Lies and colleagues grew *Shewanella* on nano-porous glass beads that contained iron oxide (Lies *et al.*, 2005). The pore size of the beads prevented direct contact between the cells and the iron oxide. Yet, *S. oneidensis* MR-1, *Shewanella* sp. ANA-3, *S. putrefaciens*, and *S. algae* BR-Y were still able to reduce the majority of the iron within the bead. In contrast, *E. coli* MG1655 reduced less than 10% of the iron (Lies *et al.*, 2005). Electrode wash-out experiments also provided evidence for a soluble mediator (Marsili *et al.*, 2008, Jiang *et al.*, 2010). In these experiments, *Shewanella* was grown as a biofilm on an electrode, and current production was measured. The media in the electrode system was replaced with fresh media, resulting in a 73-95% reduction of current production. When the original media was restored to the electrode, with planktonic cells removed, current production was restored to over 80% of the original level (Marsili *et al.*, 2008, Jiang *et al.*, 2010). Marsili and coworkers identified flavin species as the soluble mediators contributing to current production (Marsili *et al.*, 2008). To provide further evidence that flavins act as mediators of EET, *Shewanella* associated electrodes were supplemented with additional riboflavin, resulting in increased current production (Marsili *et al.*, 2008).

Indirect EET, mediated by flavin shuttles, contributes upwards of 70% of current production (Kotloski and Gralnick, 2013). In the indirect pathway (shown in Figure 1), the cell exports flavin adenine nucleotide (FAD) to the periplasm through an inner membrane multidrug and toxin efflux transporter, Bfe (Kotloski and Gralnick, 2013). In the periplasm, FAD is cleaved to flavin mononucleotide (FMN) and adenosine (AMP) monophosphate by multifunctional 5'-nucleotidase, UshA (Covington *et al.*, 2010). FMN then exits the cell, where it can be hydrolyzed to riboflavin, which is also redox-active (Covington *et al.*, 2010, Marsili *et al.*, 2008). Extracellular cytochromes, like the MtrCAB complex deposit electrons onto the flavins (Coursolle *et al.*, 2010). Coursolle and coworkers found that flavin reduction and final current production were reduced in a mutant strain of *S. oneidensis* lacking Mtr complex proteins; they estimated the Mtr pathway contributes 90% of flavin reduction activity (Coursolle *et al.*, 2010). Once flavin species are reduced by extracellular cytochromes, they can deposit electrons onto the extracellular electron acceptor. Flavin shuttles can be recycled; flavins that have deposited

electrons onto the terminal electron acceptor can be re-reduced by the MtrCAB complex and continue to shuttle electrons to the insoluble electron acceptor (Coursolle *et al.,* 2010).

Using flavin shuttles for respiration allows *Shewanella* to access insoluble electron acceptors from which they are spatially or physically separated. This ability provides a survival advantage. For example, cells confined in a biofilm that cannot directly contact an extracellular electron acceptor could still respire (Kotloski and Gralnick, 2013). While use of flavin shuttles provides clear benefits, questions remain about *Shewanella's* control of flavin composition. Flavin composition is comprised of 65% FMN and 35% riboflavin in wild-type culture supernatants (Covington *et al.,* 2010). In contrast, riboflavin predominates MR-1 and MR-4 electrode associated biofilms, making up approximately 90% of the total flavin concentration (Kotloski and Gralnick, 2013). Covington and colleagues found that in a *Shewanella* mutant strain lacking UshA, FAD, rather than FMN or riboflavin made up the majority of the flavins isolated from the supernatant (Covington *et al.,* 2010). While the flavin composition in the mutant supernatants shifted, total flavin concentration did not. Additionally, the rate of EET in the mutant measured by the rate of iron oxide reduction did not significantly differ from wild type. These data suggest that FAD, FMN, and riboflavin can all act as electron shuttles. Why then, does *S. oneidensis* cleave FAD and export FMN?

As shown in Figure 1, UshA is the enzyme responsible for the cleavage of FAD in the periplasm. UshA is a periplasmic, 5'nucleotidase (Pinchuck *et al.,* 2008), which allows *S. oneidensis* MR-1 to grow on AMP, CMP, and GMP as the sole source of carbon (Covington *et al.,* 2010). In the oligotrophic, aquatic environments where *Shewanella* lives, nutrients are limited (Pinchuck *et al.,* 2008). However, extracellular DNA is often present, providing a source of carbon, phosphate, and nitrogen. According to Pinchuck and coworkers, the concentration of extracellular DNA in water columns and sediments often exceeds that of inorganic phosphate (Pinchuck *et al.,* 2008). To exploit DNA as a nutrient source, MR-1 uses endonucleases and exonucleases to break down DNA to individual nucleotides. UshA, then cleaves the phosphate of the nucleoside moiety, so that the nucleoside can be imported into the cytosol (Pinchuck *et al.,* 2018). Covington and coworkers proposed that cleavage of FAD by UshA could be advantageous because it allows for the re-uptake of AMP. Both FAD and FMN are redox active molecules that can function as electron shuttles. Exporting FMN, rather than FAD as the primary flavin species would allow MR-1 to retain additional carbon (Covington *et al.,* 2010).

S. oneidensis UshA (SO-UshA) shares approximately 50% amino acid identity with *E. coli* UshA (EC-UshA) (Covington *et al.,* 2010). Because the structure, mechanism of action, and

substrate profile of EC-UshA are well characterized, EC-UshA serves as the foundation for our understanding of the UshA protein family within Gammaproteobacteria. (Knofel and Strater, 1999, 2001a, 2001b, Alves-Pereira *et al.,* 2008). Like SO-UshA, EC-UshA is localized in the periplasm and cleaves nucleotides AMP and CMP at a high rate (Knofel and Stater 1999, Alves-Pereira *et al.,* 2008, Covington *et al.,* 2010). However, SO-UshA hydrolyzes FAD at a much higher rate than EC-UshA (Covington *et al.,* 2010, Alves-Pereira *et al.,* 2008). *E. coli* also does not perform EET (Lies *et al.,* 2005). Because we believe FAD cleavage activity may help reduce the metabolic burden of electron shuttling in *Shewanella,* we wanted to understand the structural differences between SO-UshA and EC-UshA responsible for the higher rate of FAD cleavage in SO-UshA. The overall goal of this work is to establish a foundational understanding of the protein function of SO-UshA to further our understanding of flavin shuttling and EET.

CHAPTER 2:

The Effect of Binding Pocket Residues on *S. oneidensis* UshA FAD Cleavage Activity

INTRODUCTION

S. oneidensis MR-1 is a dissimilatory, metal-reducing bacteria capable of respiring over twenty electron acceptors (Hau and Gralnick, 2007). This huge diversity in respiratory ability could be harnessed in a number of biotechnological applications from bioremediation of toxic metals to microbial fuel cells to microbial electrosynthesis (Zou *et al.*, 2019). Many of these applications specifically take advantage of MR-1's extracellular electron transport (EET) pathway, in which electrons harvested from oxidation of carbon sources in the cytosol are transferred through the periplasm and out of the cell, where they are deposited onto an extracellular terminal electron acceptor (Hau and Gralnick, 2007).

S. oneidensis has two interacting pathways responsible for EET: a direct pathway in which electrons travel through a series of multi-heme cytochromes and an indirect pathway mediated by flavin electron shuttles (Gralnick 2012, Breuer *et al.*, 2014, Coursolle *et al.*, 2010). The indirect pathway contributes over 70% of EET, as measured by current production (Kotloski and Gralnick, 2013). In the indirect pathway, *S. oneidensis* synthesizes flavin adenine dinucleotide (FAD) in the cytosol and exports it into the periplasm through the transporter, Bfe (Kotloski and Gralnick, 2013). In the periplasm, 5'-nucleotidase UshA, cleaves FAD into FMN and AMP. UshA further cleaves AMP into adenosine and inorganic phosphate, allowing the adenosine to be transported back into the cytosol as a source of carbon and phosphorous (Covington *et al.*, 2010). FMN, however, is exported from the cell, where it is thought to be reduced by the outer membrane cytochrome complex, MtrCAB (Marsili *et al.*, 2008, Coursolle *et al.*, 2010). Reduced flavin shuttles then deposit electrons onto the terminal electron acceptor. The indirect pathway allows *S. oneidensis* to respire electron acceptors from a distance (Coursolle *et al.*, 2010).

It is not currently known whether cleavage of FAD by UshA is necessary for flavin maturation or if FAD cleavage is incidental to 5'-nucleotidase scavenging. It is known that UshA allows the cells to access the phosphate, carbon, and nitrogen in DNA, which is a useful strategy for life in aquatic, oligotrophic environments where the concentration of extracellular DNA sometimes exceeds the concentration of inorganic phosphate (Pinchuck *et al.*, 2018). Both FMN and FAD have been shown to act as electron shuttles (Covington *et al.*, 2010). Thus, UshA may not be required for effective shuttling. However, Covington and colleagues hypothesize that

UshA cleavage of FAD reduced the metabolic burden of shuttling by allowing for the reuptake of adenosine (Covington *et al.*, 2010). To better understand the role of UshA in flavin shuttling, we wanted to understand the structural basis for FAD cleavage in *S. oneidensis* MR-1 UshA (SO-UshA).

UshA is part of a large, widely-distributed multifunctional protein family of 5'nuclotidases/UDP-glucose hydrolases. Of these, *E. coli* UshA (EC-UshA) has been well characterized. EC-UshA has been crystalized, and the structure and mechanism of the enzyme has been established (Knofel and Starter, 1999, 2001a, 2001b). Briefly, EC-UshA is a metalloenzyme with two globular subunits connected by an alpha helix (Knofel and Stater, 1999). The N-terminal domain contains the catalytic asp-his dyad and the residues that coordinate the two divalent metal co-factors, while the C-terminal domain contains residues responsible for substrate binding and specificity. Notably, Phe429 and Phe498 bind the substrates' nucleoside moiety while the positively charged Arg375, 379, and 410 coordinate the phosphate groups (Knofel and Stater, 2001a, Krug *et al.*, 2013). Expressed alone, the C-terminal domain has no catalytic activity (Krug *et al.*, 2013). EC-UshA assumes two conformations, the "open" inactive conformation, and the "closed," active conformation. Substrate binds to the C-terminal in the "open" conformation. To bring the C-terminal-bound substrate into position for cleavage by the N-terminal active site residues, the protein undergoes a 96 degree "ball and socket" rotation (Knofel and Strater, 2001b). The rotation of the enzyme is likely crucial for substrate binding and release. The mechanism and active site residues described above are thought to be highly conserved within the protein family (Knofel and Stater, 1999, 2001a).

As shown in Figure 2, FAD is a much larger molecule than AMP. We hypothesized that due to the larger size of FAD, the structure of the binding pocket of SO-UshA may differ from that of EC-UshA to accommodate the larger substrate. To explore this hypothesis, we first modeled the structures of SO-UshA to identify differences in the active site binding pockets of EC-UshA versus SO-UshA. Two binding pocket residues were identified that differed between SO-UshA and EC-UshA: Arg53/His45 and Asn412/Ser405. Point mutations were then introduced into both SO-UshA and EC-UshA to change the residues in the identified positions to the identity of the residue in the corresponding position of the other enzyme. We then tested the effect of specific binding pocket residues on the rate of FAD cleavage and found that Arg in position 53/45 for SO-UshA and EC-UshA, respectively resulted in higher rates of FAD cleavage. We also characterized the FAD cleavage activity of other closely-related UshA homologs to determine whether FAD cleavage correlated with the identity of the residues in the putative binding-pocket.

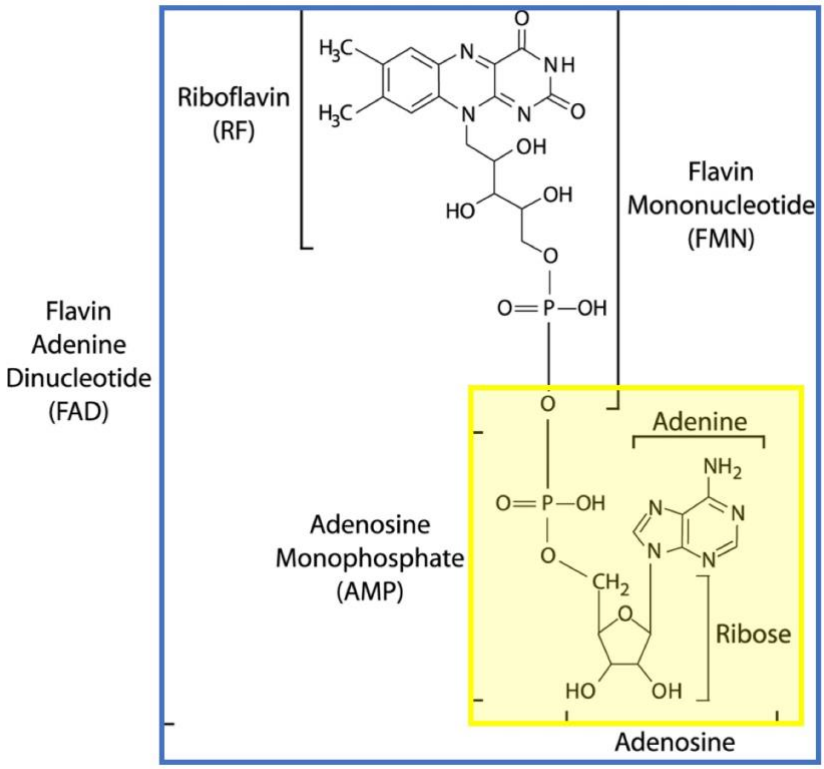

Figure 2: Structure of FAD, from Covington *et al.*, 2010, with FMN, riboflavin and AMP moieties labeled. Blue and yellow boxes added to highlight the difference in size of FAD (blue) vs AMP (yellow).

METHODS

Homology Modeling

To model the structure of *S. oneidensis* MR-1, the protein sequence of SO-UshA$_{WT}$ (UniProt ID Q8EFH1-1) was used as the sequence input in SWISS-MODEL (Waterhouse *et al.* 2018, Guex *et al.*, 2009, Bienert *et al.*, 2017, Benkert *et al.*, 2011, Bertoni *et al.*, 2017**)** with no template specified**.** Because we were interested in the differences of the active conformation binding pockets of SO-UshA versus EC-UshA, target-template alignment was also conducted in SWISS-MODEL using *E. coli* UshA in the "closed" conformation co-crystalized with ADP analog, AMPCP (Protein Data Bank ID 1HPU) (Knofel and Strater, 2001a). The resultant SO-UshA models were overlaid with their template in Edu MacPyMOL (v1.7.4) to identify and compare binding pockets residues.

Bacterial Strains and Culture Conditions

Shewanella and *E. coli* strains were struck onto Luria-Bertani (LB) agar from -80°C glycerol stocks and incubated at 30°C for *Shewanella* strains or 37°C for *E. coli* strains. All overnight cultures were inoculated with a single colony and grown in LB broth at the respective temperature for the strain, 200 rpm. Media was supplemented with 50 µg/mL kanamycin where necessary to maintain plasmids. For certain cloning and transformation steps, media was also supplemented with X-gal for blue-white screening and diaminopimelic acid (DAP) for growth of auxotrophic *E. coli* WM3064. RB media, which was used as a recovery media following chemical transformation is comprised of 10.0 g tryptone, 5.0 g NaCl, 5.0 g yeast extract, 2 mL 1 M NaOH, and 4.93 g, $MgSO_4 \cdot 7H2O$. *Shewanella* Basal Media contains 0.225 g K_2HPO_4, 0.225 g, KH_2PO_4, 0.46 g NaCl, 0.225 g $(NH_4)SO_4$, 0.117 g $MgSO_4 \cdot 7H2O$, 2.38 g HEPES per liter of ddH2O, adjusted to pH 7.2. AMP media is prepared by combining SBM, 0.5 M AMP, and 100X vitamin/mineral/1% casamino acid solution to a final AMP concentration of 10 mM and 1X vitamin/minerals/0.01% casamino acids. Phosphate-free SBM and AMP media are made without K_2HPO_4 and KH_2PO_4, all other ingredients the same as previously described. 100X vitamin/mineral mix contained 0.75 g nitriloacetic acid, 1.5 g $MgSO_4 \cdot 7H2O$, 0.25 g $MnSO_4 \cdot H_2O$, 0.5 g NaCl, 0.05 g $FeSO_4 \cdot 7H_2O$, 0.05 g $CaCl_2 \cdot 2H_2O$, 0.05 g $CoCl_2 \cdot 6H_2O$, 0.065 g $ZnCl_2$, 0.005 g $CuSO_4 \cdot 5H_2O$, 0.005 g $AlK(SO_4)_2 \cdot 12H_2O$, 0.005 g H_3BO_3, 0.0125 g Na_2MoO_4, 0.012 g $NiCl_2 \cdot 6H_2O$, 0.0125 g $Na_2WO_4 \cdot 2H_2O$, 0.001 g biotin, 0.001 g folic acid, 0.005 g pyridoxine HCl, 0,0025 g thiamine, 0.0025 g nicotinic acid, 0.0025 g pantothenic acid, 0.00005 g B-12, 0.0025 g p-aminobenzoic acid, and 0.0025 g thioctic acid per liter.

Table 1. Strains Used in Chapter 2

Strain or Plasmid	Description	Reference
E. coli strain UQ950	DH5α host for cloning: F-*(argF-lac)169 80dlacZ58(*M15*) glnV44(*AS*) rfbD1 gyrA96(*NalR*) recA1 endA1 spoT1 thi-1 hsdR17 deoR pir+*	Saltikov and Newman, 2003
E. coli strain WM3064	DAP auxotroph used for conjugation: *thrB1*004 *pro thi rpsL hsdS lacZM15* RP4-1360 *(araBAD)567 dapA*1341::[*erm pir(wt)*]	Saltikov and Newman, 2003
JG1079	*S. oneidensis* Δ*ushA*	Covington, 2010

JG1175	*S. oneidensis* Δ*ushA*: empty pBBR1_MCS2 vector	Covington, 2010
JG4308	*S. oneidensis* Δ*ushA*: SO-$ushA_{WT}$	This work
JG4311	*S. oneidensis* Δ*ushA*: SO-$ushA_{R53H}$	This work
JG4314	*S. oneidensis* Δ*ushA*: SO-$ushA_{N412S}$	This work
JG4317	*S. oneidensis* Δ*ushA*: SO-$ushA_{R53H\&N412S}$	This work
JG4319	*S. oneidensis* Δ*ushA*: EC-$ushA_{WT}$	This work
JG4322	*S. oneidensis* Δ*ushA*: EC-$ushA_{H45R}$	This work
JG4324	*S. oneidensis* Δ*ushA*: EC-$ushA_{S405N}$	This work
JG4325	*S. oneidensis* Δ*ushA*: *S. loihica* PV-4 *ushA* (SL-*ushA*)	This work
JG4326	*S. oneidensis* Δ*ushA*: *S. balitica* OS155 (SB-*ushA*)	This work
JG4327	*S. oneidensis* Δ*ushA*: *Vibrio natriegens* (VN-*ushA*)	This work
JG4328	*S. oneidensis* Δ*ushA*: *Enterobacter cloacae* e1202 *ushA* (EN-*ushA*)	This work
JG4329	*S. oneidensis* Δ*ushA*: *Serratia oryzae* J116 *ushA* (J-*ushA*)	This work
JG274	*S. oneidensis* MR-1	Venkateswaran *et al.*, 1999
JG101	*S. loihica* PV-4	Gao *et al.*, 2006
JG104	*S. balitica* OS155	Ziemke *et al.*, 1998
ATCC 14048	*Vibrio natriegens*	Payne, 1958

Strain Construction

To obtain wild-type *ushA* amplicons, colony PCR with *ushA*-specific primers was performed on the source strain or synthesized as a gBlock (Integrated DNA Technologies: Coralville, IA). For mutant SO*ushA* and EC*ushA* strains, point mutations were made to wild-type SO-*ushA* and EC-*ushA* by overlap-extension polymerase chain reaction (PCR). Using the wild-type amplicon, gene fragments upstream and downstream of the desired mutation site were amplified with primers containing the target mutation. The upstream and downstream fragments were then rejoined with overlap extension PCR (Ho *et al.*, 1989). The SO-*ushA* double mutant was made sequentially. Mutated and wild-type amplicons were restriction digested with the necessary restriction enzymes (New England Biolabs: Ipswich, MD, see supplemental for specific

enzyme), and ligated into double digested plasmid with T4 DNA ligase rapid ligation kit (Thermo Scientific: Waltham, MA).

For *S. oneidensis* Δ*ushA* complement strains, broad-range host vector pBBR1_MCS2 was used as the vector backbone (Kovach *et al.*, 1995). pBBR1_MCS2 carries a kanamycin resistance cassette and *lacZ*, allowing for blue-white screening of successfully cloned mutants (Kovach *et al.*, 1995). Mutant and wild-type genes were ligated into pBBR1_MCS2 with the appropriate directionality so the genes were under the control of the lac promoter on the plasmid. Ligation products were cloned into rubidium-competent *E. coli* UQ950. First, competent cells were thawed on ice. Ligation reaction was added, and cells were incubated on ice for 20 minutes. Cells were then heat-shocked at approximately 42°C for 45-60 seconds. Samples were then incubated on ice for 2 minutes. One mL RB media was added to each sample, and samples were allowed to recover at 37°C, 200rpm.

Cells were then plated on media supplemented with X-gal for blue-white screening. White colonies were selected, PCR screened, and saved as plasmid production strains. Plasmids were purified from the plasmid production strains with Monarch plasmid mini-prep kit (New England Biolabs: Ipswich, MD) and were then transformed into the mating strain, *E. coli* WM3064, by the same transformation procedure. *E. coli* WM3064 were then cross-streaked with *S. oneidensis* Δ*ushA* on media supplemented with diaminopimelic acid (DAP) to transfer the plasmid to the *S. oneidensis* knock-out strain. Cells from the cross-streak were then transferred to media without DAP to isolate the successfully complimented *S. oneidensis* strain from the mating strain.

AMP Growth and Cleavage Assays

For AMP growth, 1 mL of overnight LB cultures, grown in triplicate, were centrifuged at 8000rpm (6797 *x g*) for 3 minutes. Cells were washed twice with SBM, then normalized to and optical density (OD) of one to roughly control for cell concentration. One OD cells were diluted 1:100 in AMP media, and incubated at 30°C, 200rpm. OD of the AMP culture tubes was measured periodically over 24 hours to track the growth rate. Experiments were performed in triplicate for each set of strains.

For AMP cleavage, triplicate overnight cultures were washed and resuspended as before but with phosphate-free SBM. AMP cleavage rate was determined by measuring the resulting increase of inorganic phosphate by a colorimetric assay adapted from Kyaw *et al.* (1984). Briefly, 20 μL cells were combined with 5 mM AMP in SBM, mixed and then 45 μL were immediately

combined with 15 µL 1M sulfuric acid to stop the reaction for the "zero" time point. Additional samples were taken at 10, 20 and 30 minutes. 45 µL 5% (w/v) triton-100 and 45 µL ammonium molybdate in 3N sulfuric acid was added to all samples and a standard curve of KH_2PO_4 (0 µM, 50 µM, 100 µM, 250 µM, 500 µM, and 750 µM KH_2PO_4), resulting in the formation of a yellow-colored chromophore. The intensity of the yellow color is proportional to the concentration of inorganic phosphate (Kyaw *et al.*, 1984). The method was carried out in a flat-bottom 96-well plate, read at 377nm on Spectromax plate reader. Concentration of phosphate was calculated based on the standard curve for each sample, then graphed versus time for each individual replicate. Linear best-fit line was fit to the linear portion of each of these graphs in Excel. Standard error of the mean (SEM) was also calculated. Results were based on combined data from two independent experiments.

FAD cleavage Assay

1 mL of triplicate overnight LB cultures were centrifuged at 8000 rpm (6797 *x g*) for 3 minutes. Cells were washed twice with SBM, then normalized to the same OD to roughly control for cell concentration. Cells were then added to a flat-bottom 96-well plate with FAD cleavage media, comprised of 80 µM flavin adenine dinucleotide and 1X vitamin/mineral solution (without casamino acids) in SBM (Covington *et al.*, 2010). Mutant strains were tested in three sets: SO-UshA mutants, EC-UshA mutants, and UshA homologs from other bacterial strains. *S. oneidensis* Δ*ushA*: SO-$ushA_{WT}$, *S. oneidensis* Δ*ushA*: EC-$ushA_{WT,}$ and *S. oneidensis* Δ*ushA*: empty vector strains were included as controls in the tests for each set of strains. For the SO-UshA mutant strains, 190 µM FAD cleavage media was combined with 10 µL OD_{600} 1 cells. For the other two sets of strains, 25 µL of 4 OD cells were added to 175 µM FAD cleavage media. Fluorescence was monitored on a Gemini EM or Spectromax M2 Plate reader, wavelengths were 440 nm for excitation, and 525 nm for emission. Fluorescence was measured every 5 minutes over 2-3 hours. To determine the rate of FAD cleavage, a linear best-fit line was fit to the linear portion of RFU over time for each replicate in Excel. Each slope was used to calculate the change in RFU per minute per 10 µL 1 OD cells. The individual calculated rates were averaged for all the strains. SEM was calculated. Reported results were based on three biological replicates from three independent experiments.

Phylogeny construction

To examine the relatedness of EC-UshA, SO-UshA, and related 5'NT sequences, other closely related species were selected as representatives using Williams and coworkers' phylogeny of Gammaproteobacteria as a guide (Williams *et al.,* 2010). UshA homologs were then identified in the selected species using SO-UshA protein sequence (uniprot ID Q8EFH1) as query sequence for a protein BLAST search (Altschul *et al.,* 1997 & 2005). The FAD cleavage rates of these homologs were determined experimentally, as previously described. Sequences of homologs characterized in the literature were also obtained from NCBI or UniProt and added to the alignment. All sequences were aligned with MAFFT version 7 online (default settings) (Katoh *et al.,* 2017, Kuraku *et al.,* 2013). MAFFT was selected because it was designed to account for differences in amino acid chemistry that make certain substitutions more likely than others, and it has been reported to be more accurate for aligning full protein sequences (Pais *et al.,* 2014). Positions with gaps or missing data were removed from the alignment and a maximum likelihood tree was constructed with the aligned sequences using MEGA with JTT substitution matrix, 500 bootstrap replicates (Jones *et al.,* 1992, Kumar *et al.,* 2016). FigTree v1.4.3 was used to format the tree (Drummond, 2009).

RESULTS AND DISCUSSION

Homology Modeling Identified Differences in SO-UshA versus EC-UshA Binding Pockets

When provided with the amino acid sequence of SO-UshA in automated mode, SWISS-MODEL identified two potential structure templates based on sequence identity: "5'-Nucleotidase from *E. coli*" (pdb ID: 1USH) and "Crystal structure of 5'-nucleotidase precursor from *Thermus thermophilus* HB8" (pdb ID: 2Z1A) (Waterhouse *et al.,* 2018, Guex *et al.,* 2009, Bienert *et al.,* 2017, Benkert *et al.,* 2011, Bertoni *et al.,* 2017, Knofel and Strater 1999). The SO-UshA model based on 1USH had a global model quality estimation (GMQE) of 0.75 on a scale from 0 to 1, with 1 representing the highest reliability of the model, compared to a GMQE of 0.56 for 2Z1A.

1USH represents the "open," inactive form of EC-UshA (Knofel and Strater, 1999). Because we were interested in comparing the active conformation binding pockets of EC-UshA and SO-UshA, SWISS-MODEL was also run with PDB file 1HPU, "5'-NUCLEOTIDASE (CLOSED FORM), COMPLEX WITH AMPCP," specified as the template (Waterhouse *et al.,* 2018, Guex *et al.,* 2009, Bienert *et al.,* 2017, Benkert *et al.,* 2011, Bertoni *et al.,* 2017, Knofel and Strater, 2001a). 1HPU represents the "closed," inactive form of EC-UshA crystalized with ADP-analog, adenosine 5′-(α,β-methylene)diphosphate (AMPCP). The resultant model of SO-UshA in

the active conformation had a GQME of 0.75, like the model for the "open" conformation. Figure 3 depicts the models of "open" and "closed" SO-UshA overlaid onto the respective EC-UshA template structure.

Using the model of the "closed" form of SO-UshA, 19 residues with side chains facing into the binding cleft were identified and compared with the corresponding residues in EC-UshA (see Table 2). Of the 19 residues, the identity of 2 residues differed between SO-UshA and EC-UshA: Arg53/His45 and Asn412/Ser405 (Figure 3C). These two positions were then targeted for mutagenesis in both the SO-UshA and EC-UshA backgrounds to understand their impact on FAD cleavage activity.

Table 2: Binding Pocket Residues of SO-UshA vs. EC-UshA

SO-UshA Residue#	Identity	EC-UshA Residue #
51	His	43
53	**Arg/His**	45
92	Asp	84
95	Thr	87
124	Asn	116
125	His	117
128	Asp	120
185	Ile	178
259	His	252
261	Gln	254
298	Trp	291
382	Arg	375
386	Arg	379
412	**Asn/Ser**	405
417	Arg	410
436	Phe	429
438	Asn	431
507	Phe	498
513	Asp	504

:

a)

b)

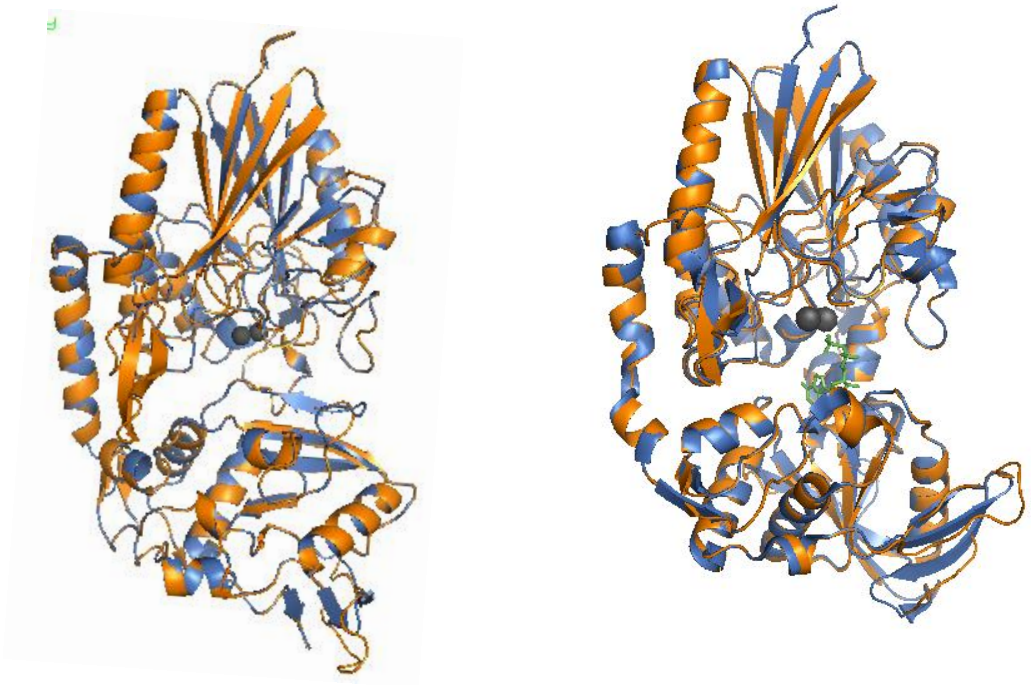

c)

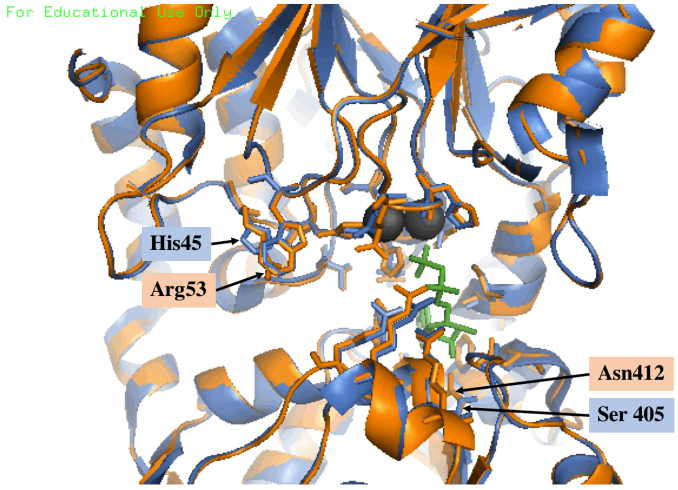

Figure 3: Overlay of EC-UshA (blue) and SO-UshA (orange). a) "open", inactive conformation and b) "closed," active conformation, shown as cartoons. In the closed conformation, the substrate, AMPCP, is depicted as sticks in green. c) Close up of the binding pocket residues with ADP analog, AMPCP. Binding pocket residues shown as blue and orange sticks for EC-UshA and SO-UshA, respectively. Of the 19 residues facing into the active binding pocket, only two differ between SO-UshA and EC-UshA. Differing residues labeled above.

R53H and N412S Mutations Reduce FAD and AMP Cleavage in SO-UshA

To test the effect of the binding pocket residues on FAD cleavage, point mutations were made in wild-type SO-*ushA* to change identity of the amino acids at position 53 and 412 to the identity of the corresponding residues in EC-UshA. *S. oneidensis* Δ*ushA* was complimented with SO-$ushA_{WT,}$ and the mutated SO-*ushA* genes: SO-$ushA_{R53H,}$ SO-$ushA_{N412S,}$ and SO-$ushA_{R53H\&N412S.}$ FAD cleavage activity was then measured for each strain. As a check to ensure the point mutations did not completely destabilize the mutant enzymes, growth rate of each strain on AMP was measured, along with the rate of AMP cleavage. AMP was selected as the control substrate because EC-UshA and SO-UshA were both expected to cleave AMP at a high rate, unlike FAD (Covington *et al.,* 2010, Alves-Periera, *et al.,* 2008). The R53H and N412S mutations were not expected to appreciably impact AMP cleavage because these two positions were hypothesized to be FAD specific.

To assess FAD cleavage, whole, stationary-phase cells were normalized to the same cell density and added to an assay solution with FAD. FAD, FMN, and riboflavin all fluoresce at the same excitation and emission wavelengths due to the aromaticity of their isoalloxazine ring (Weber 1950, Covington *et al.,* 2010). FAD, however, has a less intense fluorescent signal compared to FMN and riboflavin because of the quenching effect of its adenosine group (Weber 1950). As FAD is hydrolyzed into FMN and AMP, fluorescent signal increases. The change in relative fluorescence over time was used as the measure for the rate of FAD hydrolysis. As shown in Table 3, both the R53H and N412S mutations decrease the rate of FAD cleavage compared to SO-$UshA_{WT}$. FAD cleavage activity is even lower in the double mutant. These results suggest that the histidine and serine residues in the corresponding positions in EC-UshA may be responsible for the low rate of FAD cleavage of EC-$UshA_{WT}$. However, the rate of FAD cleavage for *S. oneidensis* ΔushA:SO-$ushA_{N412S}$ was still higher than that of the strain complimented with EC-*ushA*. This suggests that residues outside the active site binding pocket also impact substrate specificity since mutating binding pocket residues alone did not reduce activity to the level of EC-UshA.

Table 3: FAD and AMP Cleavage Rates of SO-UshA Mutants

Strain	AMP cleavage Rate (μM P_i per min per 1 OD cells)	FAD Cleavage Rate (RFU per min per 1 OD cells)

S. oneidensis Δ*ushA*: SO-*ushA*$_{WT}$	10.0 ± 0.4	53.8 ± 1.9
S. oneidensis Δ*ushA*: SO-*ushA*$_{R53H}$	4.7 ± 0.2	45.2 ± 0.1.7
S. oneidensis Δ*ushA*: SO-*ushA*$_{N412S}$	8.3 ± 0.5	37.8 ± 1.1
S. oneidensis Δ*ushA*: SO-*ushA*$_{R53N\&N412S}$	2.9 ± 0.2	21.6 ± 0.4
S. oneidensis Δ*ushA*: EC-*ushA*$_{WT}$	0.5 ± 0.2	-0.1 ± 0.4
S. oneidensis Δ*ushA*: Empty vector	0.6 ± 0.2	0.1 ± 0.1

Although a decrease in FAD cleavage activity was expected for the R53H and N412S mutations, growth rate of the strains on AMP was tested to determine whether the mutant SO-UshA proteins were still properly localized and functional. Growth on AMP is a proxy for AMP cleavage. MR-1 requires UshA for the removal of the phosphate group from AMP, which allows the adenosine moiety to be imported into the cytosol and used as a carbon source. (Covington *et al.*, 2010). To test AMP growth, cells grown overnight in LB were washed and normalized to 1 OD. These cells were then inoculated into SBM with 10 mM AMP and 1X vitamin/mineral solution with 0.01% casamino acids, and the increase in optical density of the culture was measured. Covington and colleagues had previously shown that *S. oneidensis* Δ*ushA* strains complimented with SO-*ushA* or EC-*ushA* grew with AMP as the sole carbon source at comparable rates. In contrast, complementation with EC-*ushA* was unable to restore FAD cleavage activity to the level achieved by complementation with SO-*ushA*. *S. oneidensis* Δ*ushA* complimented with an empty vector could neither grow on AMP nor restore FAD cleavage activity (Covington *et al.*, 2010). Similar to Covington and coworkers, we found that all of the complimented strains, with the exception of empty vector, grew well on AMP, as shown in Figure 4, indicating that functional SO-UshA$_{R53H,}$ SO-UshA$_{N412S,}$ and SO-UshA$_{R53H\&N412S}$ were present in the periplasm.

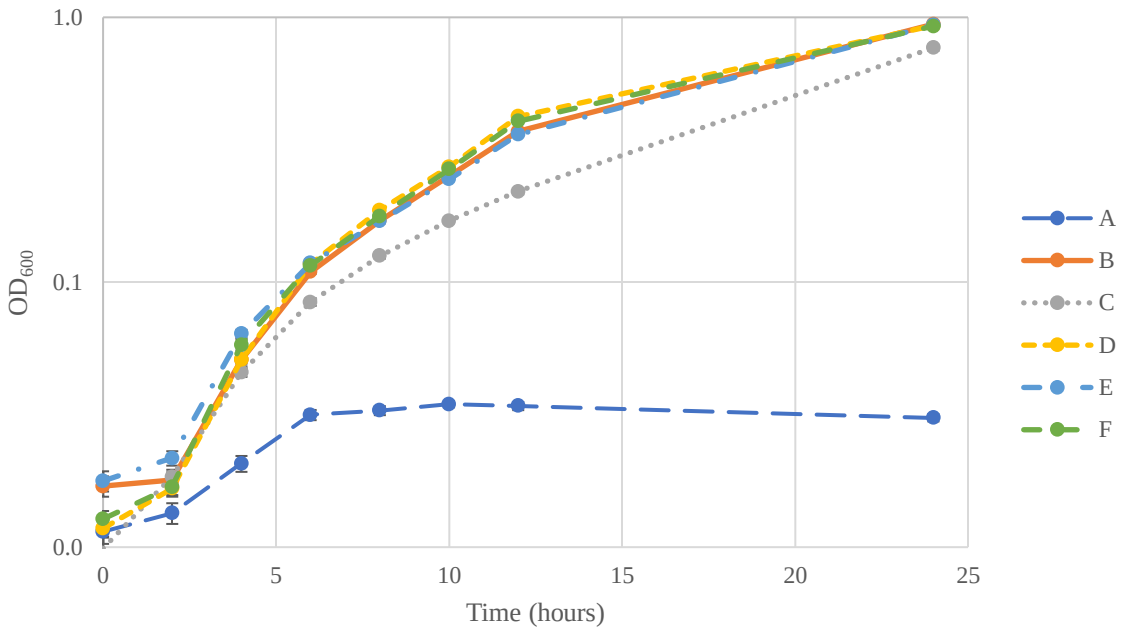

Figure 4: Growth of *S. oneidensis* Δ*ushA* complimented with A) empty vector, B) SO-*ushA*$_{WT,}$ C) EC-*ushA*$_{WT.}$ D) SO-*ushA*$_{R53H,}$ E) SO-*ushA*$_{N412S,}$ and F) SO-*ushA*$_{R53H\&N412S}$ on 10mM AMP in SBM. Growth rate for each strain represents an average of nine cultures, triplicate cultures for each of three replicate experiments. Error bars represent standard error of the mean.

Because cleavage of AMP is likely not the rate limiting step for growth on AMP, testing AMP cleavage directly provided increased resolution between activities of the SO-UshA mutants. To measure AMP cleavage, whole, stationary phase cells were washed with phosphate-free medium and incubated with AMP. At periodic time points, samples were removed and combined with 1N sulfuric acid to stop the reaction. An ammonium molybdate based assay mixture was then added to samples from each time point. Ammonium molybdate complexes with inorganic phosphate released from the cleavage of AMP, resulting in the formation of a yellow chromophore (Kyaw *et al.*, 1984). Absorbance of the samples was measured at 377 nm. Concentration of inorganic phosphate released over time was calculated based on a standard curve of KH_2PO_4. Of all the mutants, SO-UshA$_{WT}$ had the highest rate of FAD cleavage, followed by SO-UshA$_{R53H,}$ and SO-UshA$_{N412S.}$ Consistent with the FAD cleavage results, SO-UshA$_{R53H\&N412S}$ had the lowest rate of AMP cleavage activity. These results indicate that the Asn412 and Arg53 residues are important for both FAD and AMP cleavage. We had initially hypothesized that the N412S and R53H mutation would decrease FAD cleavage without impacting AMP cleavage, but this does not seem to be the case.

The AMP cleavage results also indicated there may be differences in the processing and localization of SO-UshA versus EC-UshA in the *S. oneidensis* Δ*ushA* background. Previous work with purified enzyme showed that EC-UshA had the highest activity against AMP when tested against over thirty potential substrates, including ADP, ATP, CMP, FAD, and various XDP-sugars (Alves-Pereira *et al.,* 2008). Based on the previously reported rates, it was surprising that AMP cleavage rate for *S. oneidensis* Δ*ushA*: EC-*ushA* was below the detection limit within the parameters of the assay. To our knowledge, the rate of AMP cleavage by purified SO-UshA has not been reported. While it is possible that SO-UshA has a higher FAD cleavage rate than EC-UshA, it is also possible that *S. oneidensis* Δ*ushA*: EC-*ushA* had fewer units of functional enzyme localized in the periplasm compared to *S. oneidensis* Δ*ushA*: SO-*ushA,* resulting in the lower rate of AMP cleavage observed. Although both the SO-*ushA* and EC-*ushA* genes are under the control of the same promoter, differences in protein translation and localization could affect the overall protein concentration per cell.

In the SO-UshA background, both the R53H and N412S variants reduce activity against FAD and AMP. It is possible that these mutations simply destabilize the enzyme. However, based on the AMP growth results, neither mutation destabilized the enzyme to the extent where UshA became completely nonfunctional. It is also possible that if the binding pocket residues give preference to one substrate over another, there is not a trade-off between the rate of AMP versus FAD cleavage activity. Rather, there could be a trade-off between activity against AMP and FAD versus another substrate. This is not an unreasonable hypothesis based on what is known about the C-terminal domain's control over substrate specificity in EC-UshA. The C-terminal domain binds the nucleoside moiety of the substrate (Knofel and Strater, 2001a). Both AMP and FAD have an adenosine head group. UshA enzymes are very promiscuous, binding substrates with a variety of nucleoside head groups and other moieties: mono, di, and tri-phosphate, and various sugars (Alves-Pereira *et al.,* 2018). The binding pocket residues alone may not distinguish between different substrates with the same nucleoside. Instead, differences in binding pocket residues may result in higher rates for substrates with different nucleosides.

H45R Mutation Increases FAD and AMP Cleavage in EC-UshA

Reciprocal mutations were made in the EC-UshA background. The mutant EC-*ushA* genes were then complimented into *S. oneidensis* Δ*ushA*. AMP growth and FAD cleavage were assessed by the methods described previously. The results of the experiment showed that H45R mutation increased the rate of FAD cleavage, while the S405N mutation did not. As shown in

Table 4, *S. oneidensis* Δ*ushA*: EC-$ushA_{H45R}$ showed approximately double the relative rate of FAD cleavage to 0.016 ± 0.005 RFU min^{-1} $1OD^{-1}$ compared to 0.08 ± 0.002 RFU min^{-1} $1OD^{-1}$ for *S. oneidensis* Δ*ushA*: EC-$ushA_{WT.}$ *S. oneidensis* Δ*ushA*: EC-$ushA_{S405N}$ had a slightly lower FAD cleavage rate than *S. oneidensis* Δ*ushA*: EC-$ushA_{WT.}$ The increase in FAD cleavage due to the H45R mutation in the EC-UshA background, taken with the decrease in activity due to the R53H mutation to SO-UshA, indicates that an arginine residue at this position is important for FAD cleavage activity. While the H45R mutation to EC-UshA did seem to increase FAD cleavage, the rate was still dramatically lower than that of *S. oneidensis* Δ*ushA*: SO-$ushA_{WT.}$ This suggests that other factors, such as residues outside the binding pocket or protein processing also impact enzyme activity against FAD in this experimental set up.

Unlike the SO-UshA mutants, which displayed similar growth pattern on AMP compared to SO-$UshA_{WT,}$ *S. oneidensis* Δ*ushA*: EC-$ushA_{H45R}$ and *S. oneidensis* Δ*ushA*: EC-$ushA_{S405N}$ differed from the growth pattern of *S. oneidensis* Δ*ushA*: EC-$ushA_{WT.}$ As shown in Figure 5, the H45R mutation seemed to increase growth on AMP while the S405N mutation seemed to slightly decrease growth rate. Because the S405N mutation seemed to reduce the activity against both FAD and AMP, the double mutant was not constructed in the EC-UshA background. AMP growth is a proxy for AMP cleavage, but it is not a direct measurement. The growth results may indicate that that the H45R mutation increases activity against AMP, as well as FAD. This is consistent with the decrease in both AMP and FAD due to the R53H mutation in SO-UshA. However, AMP cleavage should be measured directly to confirm an increase in activity against AMP.

Table 4: FAD and AMP Cleavage Rates of EC-UshA Mutants

Strain	FAD Cleavage Rate (RFU per min per 1 OD cells)
S. oneidensis Δ*ushA*: SO-$ushA_{WT}$	28.7 ± 0.91
S. oneidensis Δ*ushA*: EC-$ushA_{WT}$	0.08 ± 0.002
S. oneidensis Δ*ushA*: EC-$ushA_{H45R}$	0.016 ± 0.005
S. oneidensis Δ*ushA*: EC-$ushA_{S405N}$	0.06 ± 0.002
S. oneidensis Δ*ushA*: empty vector	-0.01 ± 0.000

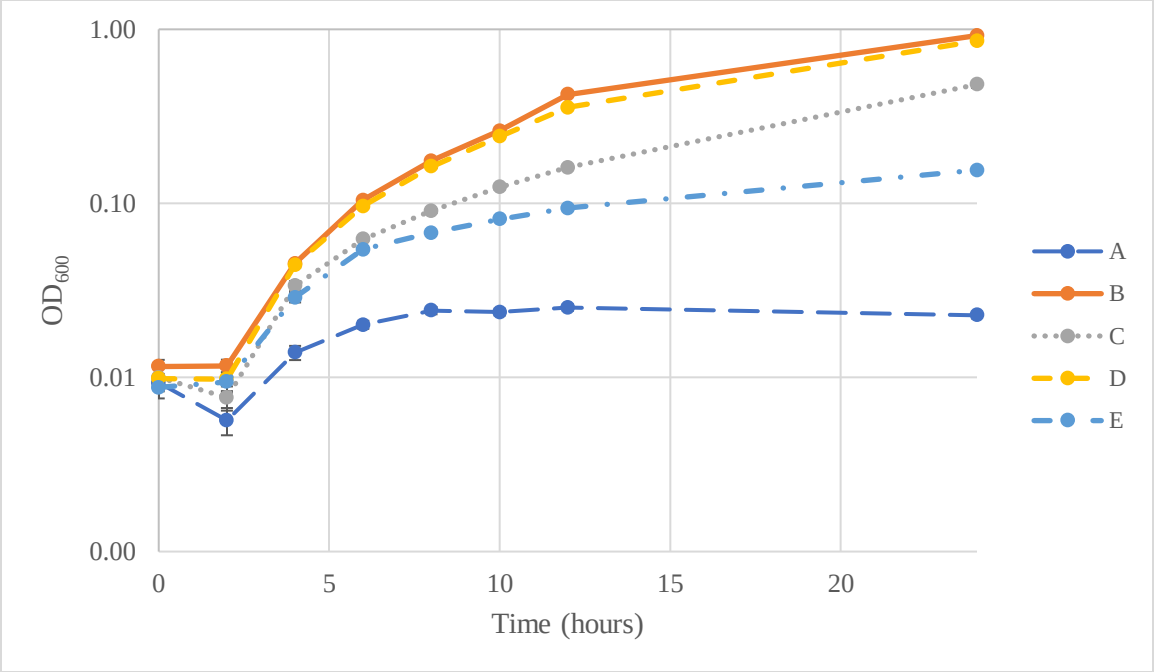

Figure 5: Growth of *S. oneidensis* Δ*ushA* complimented with A) empty vector, B) SO-*ushA*$_{WT,}$ C) EC-*ushA*$_{WT,}$ D) EC-*ushA*$_{H45R,}$ and E) SO-*ushA*$_{S405N,}$ on 10mM AMP in SBM. Growth rate for each strain represents an average of nine cultures, triplicate cultures for each of three replicate experiments. Error bars represent standard error of the mean.

These data support the idea that FAD and AMP cleavage are not in a direct trade-off with one another based on the identity of the binding pocket residues. Because the R53H mutation resulted in loss of activity of FAD and AMP in SO-UshA background, and the reciprocal H45R mutation increased AMP growth and FAD cleavage in the EC-UshA background, Arg53 is likely important for both FAD and AMP cleavage. Because both SO and EC-UshA cleave AMP at a high relative rate, we originally hypothesized that the rate of AMP would be unchanged by mutations in the binding pocket while the rate of FAD would be impacted. However, activity against both FAD and AMP seemed to be affected. Based on these data, it seems that the binding pocket is not responsible for the differences in the rate of FAD versus AMP cleavage in SO-UshA versus EC-UshA. Rather, larger-scale enzyme mechanics may be responsible for the differences in FAD cleavage between SO-UshA and EC-UshA.

This is further supported by the magnitude of the rate difference between *S. oneidensis* Δ*ushA*: SO-*ushA*$_{WT}$ and *S. oneidensis* Δ*ushA*: EC-*ushA*$_{H45R}$. Although the H45R mutation increased the rate of FAD cleavage compared to EC-UshA$_{WT}$, the FAD cleavage rate of *S. oneidensis* Δ*ushA*: EC-*ushA*$_{H45R}$ did not come close to *S. oneidensis* Δ*ushA*: SO-*ushA*$_{WT}$,

suggesting the overall structure and dynamics of SO-UshA have a larger impact on FAD cleavage than the binding pocket residues alone. To fully understand how SO-UshA protein structure drive activity against FAD, residues outside of the binding pocket require further consideration.

Knofel and Strater established that EC-UshA function depends on the rotation of the N-terminal and C-terminal domains relative to each other (Knofel and Strater, 1999, 2001b). Upon substrate binding, the domains rotate 96° relative to the "open" conformation due to a bend in the alpha helix connecting the two domains (Knofel and Strater, 2001b). Knofel and Strater identified residues 352 to 364 as the "bending residues" in the alpha helix that allow for the rotation. In the closed conformation, a "kink" forms in the alpha helix between Lys355 and Gly356. This kink is responsible for the "principal main chain torsion angle" (Knofel and Strater, 2001b). Lys355 and Gly356 are highly conserved in the UshA protein family, including in SO-UshA. However, within the "bending residues" of the alpha helix, the identity of 7 of 13 residues differ between EC-UshA and SO-UshA (Residues EC/SO: F352/Y359, N354/E361, K357/Q364, Q359/K366, E361/D368, V362/E369, and K363/V370) (Knofel and Strater, 2001b). The identity of the bending residues could impact the domain rotation angle and change the molecular dynamics of the enzyme. Although the alpha helix residues may not directly interact with the substrate, they may impact substrate specificity.

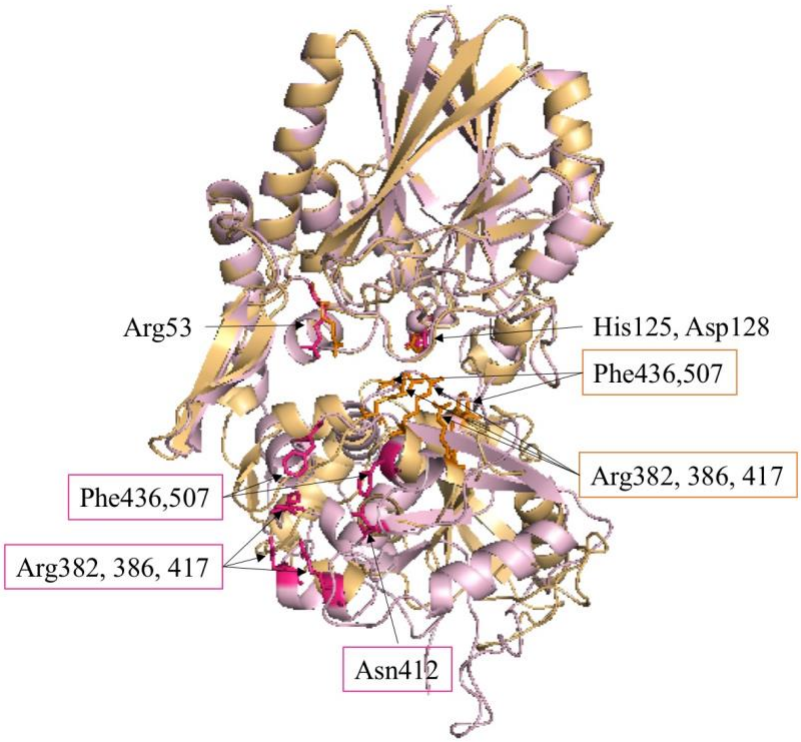

Figure 6: Models of SO-UshA in the "open" (pink) and "closed" (orange) forms depicted as cartoons. Selected residues thought to impact substrate binding shown as sticks to highlight the dynamics of the enzyme.

Our experimental analysis also dealt only with the substrate and enzyme interactions in the active, "closed" conformation. Knofel and Strater proposed that while the 96° domain rotation may be the largest domain movement, the mechanics of the enzyme involve "more complex movement consisting of small rotations around different axis" (Knofel and Strater, 2001b). The "open" and "closed" forms of the enzyme captured by crystallization are likely the two most energetically favorable conformations of the enzyme, shown in Figure 6. However, the enzyme assumes many other transitional conformations, in which other residues outside of the active site and alpha helix may ultimately impact substrate specificity. Flexibility of the enzyme scaffold could differ as well, allowing for accommodation of larger substrates. It is also notable that the H45R mutation increased AMP cleavage in EC-UshA. Previous work describing EC-UshA determined that the C-terminal residues primarily control substrate binding and specificity (Knofel and Strater, 1999&2001a). Yet, position 45 belongs to the N-terminal domain, further supporting the hypothesis that the binding pocket residues and interactions between the C-terminal and N-terminal domains controls substrate specificity.

Activity of UshA homologs in Gammaproteobacteria

We also wanted to understand FAD cleavage activity distribution within the UshA protein family in organisms closely related to *E. coli* and *S. oneidensis*. *E. coli* and *S. oneidensis* are both Gammaproteobacteria (Covington *et al.,* 2010, Williams *et al.,* 2010). Williams and coworkers constructed an extensive phylogenetic analysis of the Gammaproteobacteria using a multiple gene approach (Williams *et al.,* 2010). The phylogenetic analysis separated the Gammaproteobacteria into four subgroups, termed the "Entero," "VAAP," "PO," and "Basal" groups. *E. coli* fell into the Entero group with other *Enterobactales*, while *S. oneidensis* was grouped into the VAAP group along with *Vibrionales, Alteromonadales, Aeromonadales,* and *Pasteurellales* (Williams *et al.,* 2010). To understand how UshA structure and FAD cleavage activity are evolutionarily related, we identified UshA homologs distributed across the Entero and VAAP sister taxa and tested their ability to restore FAD cleavage and AMP growth in *S. oneidensis* Δ*ushA.*

UshA homologs have been previously described in the VAAP group. NutA is a 63kDa 5'-nucleotidase from *Vibrio parahaemolyticus* (Tamao *et al.,* 1999). While NutA is 60% identical to EC-UshA at the amino acid level, it has negligible UDP-sugar hydrolase activity (Tamao *et al.,* 1999). *Vibrio cholera* UshA (VC2174) has reported activity against all four 5' mononucleotides. (McDonough *et al.,* 2016). Similar to *S. oneidensis,* these enzymes cleave the phosphate groups from nucleotides, allowing for growth on nucleotides as a sole carbon source (Tamao *et al.,* 1999, Pinchuck *et al.,* 2008, McDonough *et al.,* 2016). Related 5'-nucleotidases have also been described in *Shewanella amazonensis* and *Shewanella violacea* with confirmed activity against AMP (Kuribayashi *et al.,* 2017, Fujimori *et al.,* 2019)

To test FAD cleavage activity, we complimented *S. oneidensis ΔushA* with three UshA homologs from VAAP group organisms. As representatives from the VAAP group, we selected "bifunctional UDP-sugar hydrolase/5'-nucleotidase from *Shewanella loihica* PV-4 (SL-UshA, WP_011865933.1), *Shewanella baltica* OS155 (SB-UshA, WP_011847066.1), and *Vibrio natriegens* ATCC 14048 (VN-UshA WP_020332984.1). Both *S. loihica* and *S. baltica* belong to the *Alteromonadales* group along with MR-1 (Williams *et al.,* 2010). Their UshA homologs are 78% and 85% identical to SO-UshA respectively, according to protein BLAST (Altschul *et al.,* 1997, 2005). VN-UshA was selected as a representative of the *Vibrionales* and shares 57% identity with SO-UshA. The *ushA* genes from the three organisms were amplified by colony PCR into cloned pBBR1MCS-2 and transformed into *S. oneidensis ΔushA* (Kovach *et al.,* 1995). We then tested AMP growth and FAD cleavage as before. As shown in Figure 7, SB-UshA and SL-UshA restored AMP growth to the level of SO-UshA. VN-UshA, however, did not. SL-UshA, SB-UshA, and VN-UshA all had a high rate of FAD cleavage, similar to SO-Usha (Table 5).

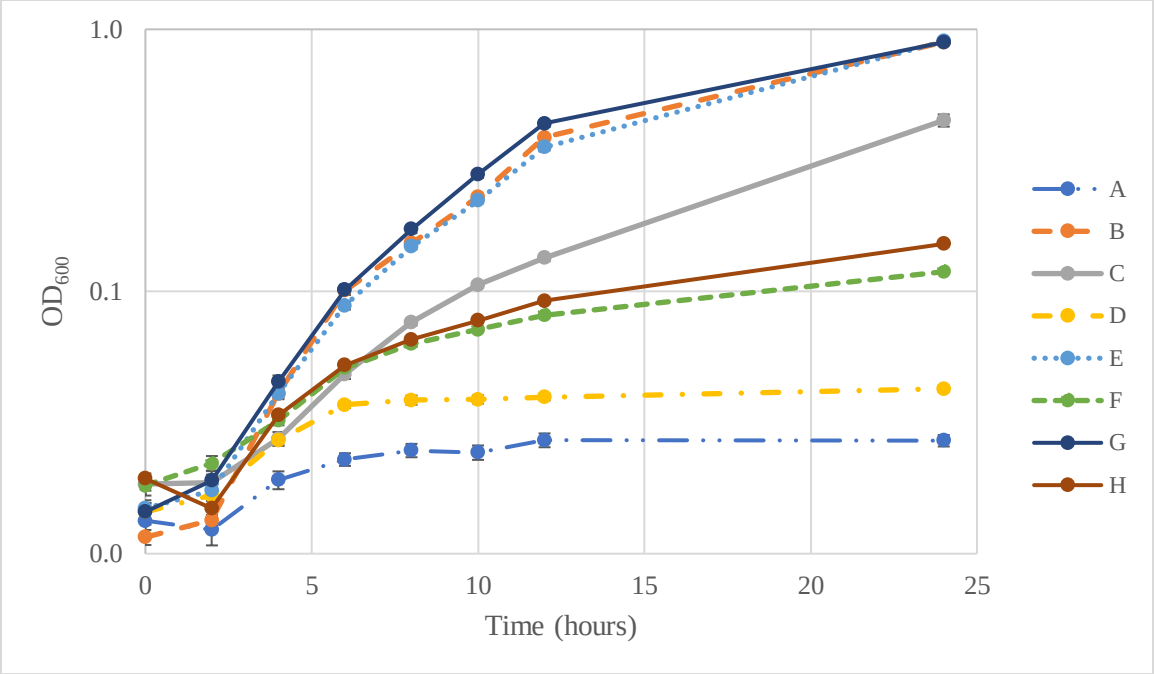

Figure 7: Growth of *S. oneidensis* Δ*ushA* complimented with A) empty vector, B) SO-$ushA_{WT,}$ C) EC-$ushA_{WT.}$ D) VN-$ushA_{WT,}$ E) SB-$ushA_{WT,}$ and F) EN-$ushA_{WT,}$ G) SL-$ushA_{WT}$, and H) J-$ushA_{WT}$ on 10mM AMP in SBM. Growth rate for each strain represents an average of nine cultures, triplicate cultures for each of three replicate experiments. Error bars represent standard error of the mean.

Table 5: FAD and AMP Cleavage Rates of *S. oneidensis* complimented with different UshA homologs.

Strain	FAD Cleavage Rate (RFU per min per 1 OD cells)
S. oneidensis Δ*ushA*: SO-$ushA_{WT}$	37.95 ± 1.08
S. oneidensis Δ*ushA*: EC-$ushA_{WT}$	0.08 ± 0.01
S. oneidensis Δ*ushA*: VN-$ushA_{WT}$	41.77 ± 0.76
S. oneidensis Δ*ushA*: SB-$ushA_{WT,}$	44.81 ± 1.07
S. oneidensis Δ*ushA*: EN-$ushA_{WT}$	0.01 ± 0.00
S. oneidensis Δ*ushA*: SL-$ushA_{WT}$	32.58 ± 1.42
S. oneidensis Δ*ushA*: J-$ushA_{WT}$	0.14 ± 0.01
S. oneidensis Δ*ushA*: Empty vector	-0.03 ± 0.00

Within the Entero group, UshA is found in most *Yersinia* species (Alves-Pereira *et al.*, 2008). EC-UshA and *Yersinia intermedia* UshA share 75% amino acid identity. Like EC-UshA,

Y. intermedia UshA cleaved AMP at a high rate, but FAD at a low rate. *Y. intermedia* UshA also has CDP-alcohol activity, which has not been reported for any other UshA homolog (Alves-Pereira *et al.,* 2008). An UshA protein with confirmed UDP-sugar hydrolase activity has been reported in *Enterobacter aerogenes* (Lee *et al.,* 2000). Other organisms in the Entero group lack functional UshA homologs. *Salmonella* strains from subgroup I, like *Salmonella typhimurium,* have the gene for *ushA,* but it contains a silencing mutation (Edwards *et al.,* 1993). *S. typhimurium* strains do have a functional CDP-sugar hydrolase, UshB. However, UshB is not evolutionarily related to UshA and does not have 5'-nucleotidase activity (Edwards *et al.,* 1993*). Yersinia pestis* has a frameshift mutation in its *ushA,* rendering the gene non-functional (Alves-Pereira *et al.,* 2008).

To sample FAD activity within the Entero group, genes for *ushA* homologs were selected from *Enterobacter cloacae* e1202 (EN-UshA: WP_063137861.1) and *Serratia oryzae* J11-6 (J-UshA WP_076940609.1). Both genes were synthesized as gBlocks, cloned into pBBR1MCS-2, and complimented into *S. oneidensis ΔushA* (Kovach *et al.,* 1995). The complimented strains' AMP growth and FAD cleavage were tested along with the strains complimented with VAAP group *ushA* homologs. EN-UshA had negligible FAD cleavage activity, while J-UshA had slightly higher FAD cleavage activity than EC-UshA (Table 5). Complementation with EN-*ushA* and J-*ushA* restored growth on AMP compared to empty vector, but not to the level of complementation with SO-$ushA_{WT}$ (Figure 7).

Based on the organisms that have been selected and described, FAD cleavage appears to have involved in certain groups. By no means are the results of this experiment comprehensive. The UshA protein family is widely distributed and includes thousands of unique proteins. In the representatives tested, VAAP group UshA homologs had a high rate of FAD cleavage, while homologs from the Entero group had little to no FAD cleavage activity. A MAFFT alignment of the protein sequences showed that SL-UshA, SB-UshA and VN-UshA also have an arginine and an asparagine at the positions corresponding to residue 53 and 412 in SO-UshA. In EN-UshA and J-UshA, the identity of residues corresponding to 45 and 405 are histidine and serine, like in EC-UshA. Per this analysis, the structure of the binding pocket and the substrate specificity seem to be evolutionarily related.

All of the enzymes were complimented into the *S. oneidensis* Δ*ushA* background under the control of the same promoter. However, differences in translation, processing, and localization could also affect the number of functional proteins per cell. As cleavage rates were normalized by cell density, differences in number of proteins per cell could impact the observed

cleavage rate. All of the UshA homologs were sourced from fairly closely-related organisms. Thus, we expected *S. oneidensis* would be able to produce and properly localize all of the UshA homologs. Based on the experimental evidence, this seemed to be the case to some extent. However, we cannot exclude the possibility that rates were impacted by differences in post-transcriptional steps in protein expression.

Interestingly, while VN-UshA had FAD cleavage activity comparable to other VAAP group UshA homologs, its compliment strain showed little to no growth on AMP. Per a BLASTp search of *V. natriegens* ATCC14048, two unique homologs of SO-UshA were found with an E value of 0.0 (Altschul *et al.*, 1997&2005). VN-UshA (WP_020332984.1), tested in this experiment, is 57% identical to SO-UshA. The alternate VN-UshA (VN-UshA$_2$: WP_020333325.1) is 55% identical to SO-UshA and only 54% identical to VN-UshA. It would be interesting for future experiments to examine whether the substrate specificities of the two UshA homologs differ and whether each protein has a unique physiological role

Broader Phylogenetic Analysis and Activity Summary

UshA homologs are also distributed in bacteria outside of the Gammaproteobacteria. One example is a 5'- nucleosidase from *Corynebacterium glutamicum*, a gram-positive bacterium. This 5'-nucleotidase has confirmed activity against GMP, IMP, AMP, CMP, UMP, ADP, ATP, and UDP-glucose (Rittmann *et al.*, 2005). Unlike in the Gammaproteobacteria, where UshA is localized to the periplasm, *C. glutamicum* excretes UshA secreted extracellularly to aid in nucleotide scavenging. UshA is expressed in phosphate starvation conditions and is required for growth on AMP and UDP-glucose as the sole phosphate source. However, *C. glutamicum* cannot use AMP as a sole carbon source (Rittman *et al.*, 2005).

Another notable example is YfkN from *Bacillus subtilis* (Chambert *et al.*, 2013). YfkN is a protein fusion of an UshA homolog and a 2'3' cyclic-nucleotidase. The protein is 143.5 kDa, the largest protein expressed by *B. subtilis*. While YfkN cleaves 5'-nuclotides such as GMP, AMP, CMP, and UMP, its activity against 2'3' cyclic nucleotides is greater than its activity against 5'nucleotides (Chambert *et al.*, 2013). When the enzyme is cleaved by the protease subtilisin, two functional protein fragments are released. One fragment retains 2'3' cyclic nucleotidase activity while the other retains 5'-nucleotidase activity, providing further evidence that this protein is a fusion (Chambert *et al.*, 2013). Like *Corynebacterium, B. subtilis* is gram-positive and secretes YfkN. Phosphate starvation drives YfkN expression (Allenby *et al.*, 2005).

Using the sequences of the UshA homologs described in Figure 7 and Table 5, as well as homologs reported in the literature, a phylogenetic tree was constructed and annotated with the relative activities against FAD, 5'-nuclotidases, and XDP-sugars. As shown in Figure 8, all of the enzymes, with the exception of VN-UshA, seemed to have activity against AMP or other 5'-nucleotides. Activity against FAD, however, seemed higher for proteins from organisms more closely related to *S. oneidensis* than those more closely related to *E. coli.*

Within the alignment, UshA homologs in *Shewanella* and *Vibrio* species have an Arg and Asn at the residues corresponding to Arg53 and Asn412 in SO-UshA while Entero group organisms have a His and Ser residue at residues aligned with His45 and Ser405 in EC-UshA. Although this binding pocket signature seems to correspond with FAD cleavage activity, other residues outside the binding pocket that evolved with VAAP versus Entero group organisms may contribute to FAD cleavage activity. To better understand this relationship, FAD cleavage activity in UshA homologs outside the Gammaproteobacteria could be characterized. Both *C. glutamicum* UshA and *B. subtilis* YfkN have a His at the position corresponding to His45, like EC-UshA, but they have Asn that aligns with Asn412, like SO-UshA. Establishing the rate of FAD cleavage activity could shed further light on the impact of the binding pocket residues and provide clues to the activity of the ancestral enzyme.

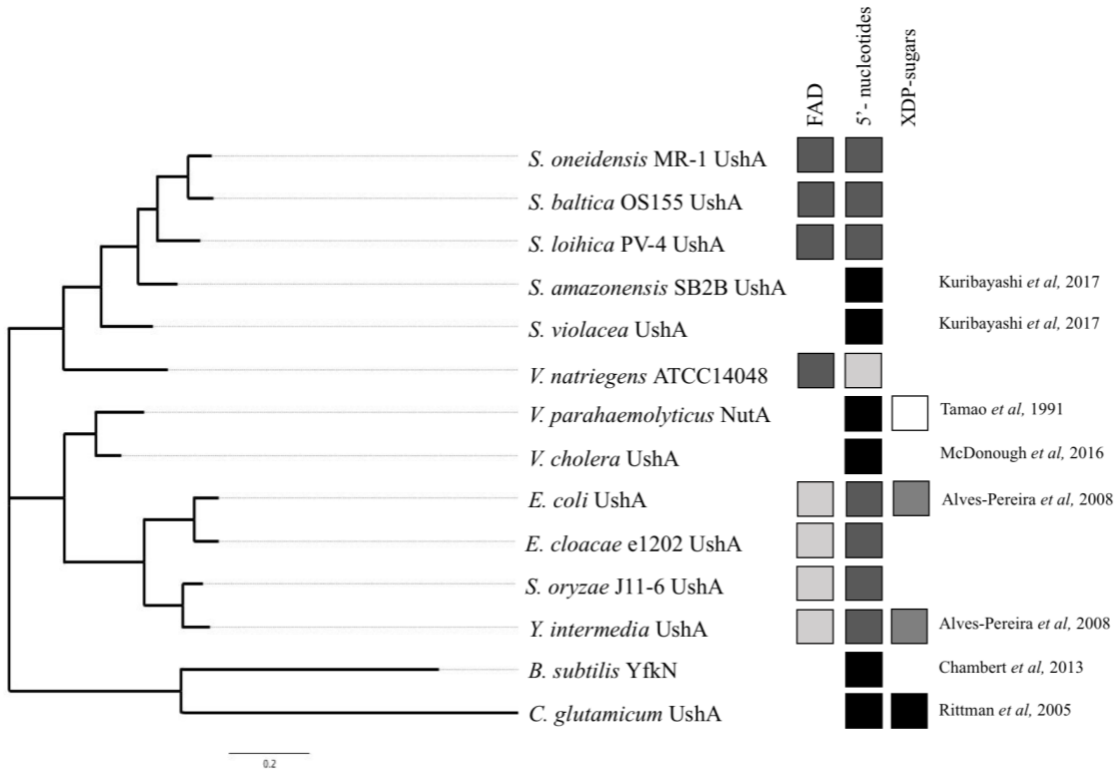

Figure 8: Phylogeny of UshA homologs: Sequences of UshA homologs from selected Gamma proteobacteria were aligned with MAFFT online and a phylogeny was constructed from the alignment using the maximum likelihood method with a JTT matrix-based model with 500 bootstrap replicates. Relative activity against FAD, 5' nucleotides, and XDP-sugars were annotated based on either the experimental data described in this work or the references specified. Shade of the box indicates relative rate of activity against the substrate, the darker shade of the box, the greater the relative activity. For references that did not specify relative rates, a black box indicates the enzyme has activity against the substrate while a white box indicates negligible activity. Lack of box indicated activity against the substrate has not been tested for the particular protein, to our knowledge.

CONCLUSION

The goal of this work was to increase our foundational understanding of SO-UshA to better understand the composition of flavin shuttles in *S. oneidensis* MR-1. Based on the results of the experiments described in this work, the binding pocket of SO-UshA impacts the rate of FAD cleavage. Arg53 seemed particularly important for activity against FAD, as the R53H mutation reduced FAD cleavage. The H45R mutation to EC-UshA increased activity, highlighting the importance of the identity of this residue. Additionally, SB-UshA, SL-UshA, and VN-UshA have both an arginine in this position and a high rate of FAD cleavage.

Asn412/Ser405 also differed between the binding pockets of SO-UshA and EC-UshA. However, mutating this residue reduced FAD cleavage in both EC-ushA and SO-UshA. The residue in this position may be supported by other residues outside the active site. Mutating this residue alone could have destabilized the enzyme, resulting in the decrease of function. These results highlight the potential impact of residues outside the binding pocket on enzyme activity. Activity against AMP and FAD were both impacted by the point mutations made to the binding pocket. Thus, residues outside the binding pocket likely contribute to the difference in the rate of FAD cleavage between SO-UshA and EC-UshA.

Changes in AMP cleavage and growth corresponded to the trends in FAD cleavage for the mutants. Enzymes in the UshA protein family have reported activities against nucleotides with various bases, XDP-sugars, and XDP-alcohols (Alves-Pereira *et al.,* 2008, Kuribayashi *et al.*, 2017, Fujimori *et al.*, 2019, Tamao *et al.*, 1999, Lee *et al.*, 2000, Rittmann *et al.*, 2005, Chambert *et al.,* 2013). Certain enzymes may have binding pockets that show preference to purines vs. pyrimidines (Rittmann *et al.*, 2005). Specificity of other homologs may depend on the size or polarity of the substrate. While we expected the mutations introduced to SO-ushA and EC-ushA would alter activity to FAD specifically, this was not the case. Instead, there could be a trade-off in activity between AMP and FAD with another substrate.

CHAPTER 3:
CONCLUSIONS AND FUTURE DIRECTIONS

This work focused on the relationship between binding pocket residues and FAD cleavage activity. To understand the full mechanisms of substrate specificity of SO-UshA, future research could examine the impact of residues outside the binding pocket. Based on previous characterization of EC-UshA, the enzyme is dynamic, and its activity depends on the movement of the N-terminal and C-terminal domains relative to one another (Knofel and Strater, 1999, 2001b). Not only does the enzyme scaffold support the binding pocket residues, it influences the position of the specificity-driving C-terminal domain relative to the catalytic residues on the N-terminal domain (Knofel and Strater, 1999, 2001b). The alpha helix connecting the N-terminal and C-terminal domains is particularly intriguing for future research because the alpha helix drives the torsion angles in the movement of the enzyme (Knofel and Strater 2001b). There are more differences in the identity of the "bending residues" between EC-UshA and SO-UshA than differences in binding pocket residues, which could impact activity.

The experiments reported in this work could be repeated *in vivo* with purified enzyme. Doing so would allow for better characterization of the enzyme mechanics of SO-UshA, EC-UshA and the mutant enzymes, as potential differences in protein concentration per cell would no longer be a factor. We determined the binding pocket residues of SO-UshA from a homology model based on the crystal structure of EC-UshA. However, obtaining the crystal structure of purified SO-UshA would confirm the structure of the binding pocket. Establishing the "open" and "closed" structures of SO-UshA could also show differences in torsion angle of protein, which may impact substrate specificity.

We were primarily interested in FAD cleavage activity because of the importance of flavins as electron shuttles in *S. oneidensis* EET. However, the UshA protein family has activity against a variety of substrates. Understanding substrate specificity for a variety of UshA homologs compared to the source organisms' living environment could provide interesting insights about different organisms' living strategies and evolutionary histories. To further understand distribution of flavin shuttling, organisms with identical binding pocket residues as SO-UshA could be tested for their ability to perform EET.

-

SUPPLEMENTARY

Table S1: Table of Primers Used

Primer Name	Sequence	Restriction Site
M13F_18mer	TGTAAAACGACGGCCAGT	NA
M13R_17mer	CAGGAAACAGCTATGAC	NA
ushA midseqDN	CTACGCCGATGGCCAAAATG	NA
ushA midseqUP	CGACCGACATACTTACCCCA	NA
ECushA midseq	TCGCTTTTCCCGTCTTCCC	NA
UshA 53 R-H 5’	ATACCAATGATAACCATGGCCATTTTTGGGAAAACAAAG ATGG	NA
UshA 53 R-H 3’	CCATCTTTGTTTTCCCAAAAATGGCCATGGTTATCATTGG TAT	NA
UshA 412 N-S 5’	CTGCTGATTTTGGGGTGATGAGCTCAGGTGGTGTGCGCGC TTC	NA
UshA 412 N-S 3’	GAAGCGCGCACACCACCTGAGCTCATCACCCCAAAATCA GCAG	NA
S405R3'	TTGCGGTGATGAACGGAGGCGGAAT	NA
S405R5'	ATTCCGCCTCCGTTCATCACCGCAA	NA
ECushA-HR-UP2	CGCCAAAAATGCCCATGAT	NA
ECushAHR-DN2	ATCATGGGCATTTTTGGCG	NA
SoUshA-5’BamHI2	AAAAGGATCCCAAGGGGTTGATGTAATGACAAATA	BamHI
SoUshA-3’XbaI2	AAAATCTAGAGAGTGGCATTTTATTAACTGCTGTA	XbaI
EcUshA-5’BamHI	AAAAGGATCC ATCAGGTCAGGGAGAGAAGT	BamHI
EcUshA-3’XbaI	AAAATCTAGATTACTGCCAGCTCACCTCA	XbaI
SL-PV_F-BamHI	AAAAGGATCCATCTAGGGGTTGATGTAAT	BamHI
SL-PV_R-SacI	AAAAGAGCTCCGCTTAATCCTGCTTATTG	SacI
SB-OS_F-BamHI	AAAAGGATCCGGTTGATGTAATGAGACATA	BamHI
SB-OS_R-SacI	AAATGAGCTCTTAAACACTGAGTAATGATTGA	SacI
E.clo_F-kpnI	AAAAGGTACCATGAAGTTAATAAAGCGTG	KpnI
E.clo_R-XbaI	AAAATCTAGACTACTGCCAGCTCACCT	XbaI
J116_KpnI_F3	AAAAGGTACCATGCGTTTTTCG	KpnI
J116_XbaI_R	AAATTCTAGATTACTGATAAACAATCTCACCT	XbaI
VN2_F-BamHI	AAAAGGATCCACAAACAAAGGTTCTACTTA	BamHI
VN2_R-SacI	AAAAGAGCTCATAAACTTCGGCTTGTAAA	SacI

REFERENCES:

Altschul SF, Madden TL, Schaffer AA, Zhang J, Zhang Z, Miller W, Lipman D. 1997. Gapped LAST and PSI-BLAST: a new generation of protein database search programs, Nucleic Acids Res. 25:3389-3402.

Altschul SF, Wootton JC, Gertz EM, Agarwala R, Morgulis A, Schaffer AA, Yu Y. 2005. Protein database searches using compositionally adjusted substitution matrices. FEBS J. 272:5101-5109.

Alves-Periera I, Canales J, Cabezas A, Cordero PM, Costas MJ, Cameselle JC. 2008. CDP-alcohol hydrolase, a very efficient activity of the 5'-nucleotidase/UDP-sugar hydrolase encoded by the *ushA* gene of *Yersinia intermedia* and *Escherichia coli*. J Bacteriol. 190(18):6153-61. doi: 10.1128/JB.00658-08.

Benker P, Biasini M, Schwede T. 2011. Toward the estimation of the absolute quality of individual protein structure models. Bioinformatics 27, 343-350.

Bertoni M, Kiefer F, Biasini M, Bordoli L, Schwede T. 2017. Modeling protein quaternary structure of homo- and hetero-oligomers beyond binary interactions by homology. Sci Rep 7.

Bienert, S., Waterhouse, A., de Beer, T.A.P., Tauriello, G., Studer, G., Bordoli, L., Schwede, T. 2017. The SWISS-MODEL Repository - new features and functionality. Nucleic Acids Res. 45, D313-D319.

Breuer M, Rosso KM, Blumberger J, Butt JN. 2015, Multi-haem cytochromes in *Shewanella oneidensis* MR-1: Structures, functions, and opportunities. J R Soc Interface. 12:20141117. doi: 10.1098/rsif.2014.1117.

Brutinel, ED, Gralnick, JA. 2011. Shuttling happens: soluble flavin mediators or extracellular electron transfer in *Shewanella*. Appl Microbiol Biotechnol. 93(1):41-48. doi: 10.1007

Bucking C, Popp F, Kerzenmacher S, Gescher J. 2010. Involvement and specificity of *Shewanella oneidensis* outer membrane cytochromes in the reduction of soluble and solid-phase terminal electron acceptors. FEMS Microbiol Lett 306; 144–151.

Chambert R, Pereira Y, Petit-Glatron MF. 2003. Purification and characterization of YfkN, a trifunctional nucleotide phosphoesterase secreted by *Bacillus subtilis*. J Biochem. 134(5):655-60 Allenby NE**,** O'Connor N, Prágai Z, Ward AC, Wipat A, Harwood CR. Genome-wide transcriptional analysis of the phosphate starvation stimulon of *Bacillus subtilis*. J Bacteriol. 187(23):8063-80

Corts, AD, Thomason LC, Gill RT, Gralnick JA. 2019. Efficient and Precise Genome Editing in Shewanella with Recombineering and CRISPR/Cas9-Mediated Counter-Selection. ACS Synth. Biol. acssynbio.9b00188 doi:10.1021/acssynbio.9b00188

Coursolle D, Baron DB, Bond DR, Gralnick JA. 2010. The Mtr respiratory pathway is essential for reducing favins and electrodes in *Shewanella oneidensis*. J of Bacteriol. 192.2: 467–474. doi:10.1128/JB.00925-09.

Covington, E.D., Gelbmann, C.B., Kotloski, N.J., Gralnick, J.A. 2010. An essential role for UshA in processing of extracellular flavin electron shuttles by *Shewanella oneidensis*. Molecular Microbiology doi:10.1111/j.1365-2958.2010.07353.x.

Drummond AJ. 2009. FigTree v1.4.3. http://tree.bio.ed.ac.uk/software/figtree/. Retrieved 10 June 2019. (Software).

Edwards CJ, Innes DJ, Burns DM, Beacham IR. 1993. UDP-sugar hydrolase isozymes in *Salmonella enterica* and *Escherichia coli*: silent alleles of *ushA* in related strains of group I *Salmonella* isolates, and of *ushB* in wild-type and K12 strains of *E. coli*, indicate recent and early silencing events, respectively. FEMS Microbiol Lett. 15;114(3):293-8.

Fujimori K, Fujii S, Lisdiana L, Wakai S, Yagi H, Sambongi Y. 2019. Differences in biochemical properties of two 5'-nucleotidases from deep- and shallow-sea *Shewanella* species under various harsh conditions. Biosci Biotechnol Biochem. 83(6):1085-1093. doi: 10.1080/09168451.2019.1578641

Gao H, Obraztova A, Stewart N, Popa R, Fredrickson JK, Tiedje JM, Nealson KH, Zhou J. Shewanella loihica sp. nov., isolated from iron-rich microbial mats in the Pacific Ocean. Int J Syst Evol Microbiol. 56(Pt 8):1911-6.

Gralnick JA. 2012. On conducting electron traffic across the periplasm. Biochem Soc Trans 40(6):1178-80. doi: 10.1042/BST20120129.

Guex N, Peitsch, MC, Schwede T. 2009. Automated comparative protein structure modeling with SWISS-MODEL and Swiss-PdbViewer: A historical perspective. Electrophoresis 30, S162-S173.

Hau HH, Gralnick JA. 2007. Ecology and biotechnology of the genus *Shewanella*. Annu Rev Microbiol. 61:237–258.

Ho SN, Hunt HD, Horton RM, Pullen JK, Pease LR. 1989. Site-directed mutagenesis by overlap extension using the polymerase chain reaction. Gene 77(1): 51-59.

Jones DT, Taylor WR, Thornton JM. 1992. The rapid generation of mutation data matrices from protein sequences. Comput Appl Biosci 8:275–282.

Katoh K, Rozewicki J, Yamada KD. 2017. MAFFT online service: multiple sequence alignment, interactive sequence choice and visualization. Brief Bioinform. doi: 10.1093/bib/bbx108

Knofel T, Strater N. 1999. X-ray structure of the *Escherichia coli* periplasmic 5'-nucleotidase containing a dimetal catalytic site. Nat Struct Biol. 6(5): 448-53. DOI: 10.1038/8253.

Knofel T, Stater N. 2001a. Mechanism of hydrolysis of phosphate esters by the dimetal center of 5'-nucleotidase Based on crystal structures. J. Mol. Biol 309, 239-254. doi:10.1006/jmbi.2001.4656

Knofel T, Stater N. 2001b. *E. coli* 5'-nucleotidase undergoes a hinge-bending domain rotation resembling a ball-and-socket motion. J. Mol. Biol 309, 255-266. doi:10.1006/jmbi.2001.4657.

Kotloski NJ, Gralnick JA. 2013. Flavin Electron Shuttles Dominate Extracellular Electron Transfer by *Shewanella oneidensis*. mBio 4(1).

Kovach ME, Elzer PH, Hill DS, Robertson GT, Farris MA, Roop RM 2nd, Peterson KM. 1995. Four new derivatives of the broad-host-range cloning vector pBBR1MCS, carrying different antibiotic-resistance cassettes. Gene. 166(1):175-6

Krug U, Patzschke R, Zebisch M, Balbach J, Sträter N. 2013. Contribution of the two domains of E. coli 5'-nucleotidase to substrate specificity and catalysis. FEBS Lett. 587(5):460-6. doi: 10.1016/j.febslet.2013.01.010.

Kumar S, Stecher G, Tamura K. 2016. MEGA7: Molecular Evolutionary Genetics Analysis version 7.0 for bigger datasets. Mol Biol Evol 33: 1870–1874.

Kuraku S, Zmasek CM, Nishimura O, Katoh K. 2013. aLeaves facilitates on-demand exploration of metazoan gene family trees on MAFFT sequence alignment server with enhanced interactivity. Nucleic Acids Res. W22-8. doi: 10.1093/nar/gkt389.

Kuribayashi TA, Fujii S, Masanari M, Yamanaka M, Wakai S, Sambongi Y. 2017. Difference in NaCl tolerance of membrane-bound 5'-nucleotidases purified from deep-sea and brackish water *Shewanella* species. Extremophiles 21(2):357-368. doi: 10.1007/s00792-016-0909-8.

Kyaw A, Maung-U K, Toe,T. 1984. Determination of Inorganic phosphate with molybdate and triton X-100 without reduction. Analytical Biochemistry 145, 230-234.

Lee KS, Song SB, Kim KE, Kim YH, Kim SK, Kho BH, Ko DK, Choi YK, Lee YK, Kim CK, Kim YC, Lim JY, Kim Y, Min KH, Wanner BL. 2000. Cloning and characterization of the UDP-sugar hydrolase gene (*ushA*) of *Enterobacter aerogenes* IFO 12010. Biochem Biophys Res Commun. 269(2):526-31

Lies DP, Hernandez ME, Kappler A, Mielke RE, Gralnick JA, Newman DK. 2005. *Shewanella oneidensis* MR-1 uses overlapping pathways for iron reduction at a distance and by direct contact under conditions relevant for Biofilms. Appl Environ Microbiol. 71(8):4414-4126.

Marsili E, Baron DB, Shikhare ID, Coursolle D, Gralnick JA, Bond DR. 2008. *Shewanella* secretes flavins that mediate extracellular electron transfer. Proc Natl Acad Sci USA 105(10):3968-73. doi: 10.1073/pnas.0710525105.

Murphy AC, 2011. Metabolic engineering is key to a sustainable chemical industry. Nat Prod Rep. 28(8):1406-25. doi: 10.1039/c1np00029b.

Pais FS, Ruy PC, Oliveira G, Coimbra RS. 2014. Assessing the efficiency of multiple sequence alignment programs. Algorithms Mol Biol 9(1):4. doi: 10.1186/1748-7188-9-4.

Payne WJ. 1958. Studies on bacterial utilization of uronic acids. III. Induction of oxidative enzymes in a marine isolate. J Bacteriol. 76(3):301-7.

Pinchuk GE, Ammons C, Culley DE, Li SM, McLean JS, Romine MF, Nealson KH, Fredrickson JK, Beliaev AS. 2008. Utilization of DNA as a sole source of phosphorus, carbon, and energy by *Shewanella* spp.: ecological and physiological implications for dissimilatory metal reduction. Appl Environ Microbiol. 74(4):1198-208.

Rittman D, Sorger-Herrman U, Wendisch VF. 2005. Phosphate starvation-inducible gene *ushA* encodes a 5' nucleotidase required for growth of *Corynebacterium glutamicum* on media with nucleotides as the phosphorus source. Appl. Environ. Microbiol. 71(8):4339-44.

Saltikov CW, Newman DK. 2003. Genetic identification of a respiratory arsenate reductase. Proc. Natl. Acad. Sci. U. S. A. 100:10983-10988.

Scheutz B, Schicklberger M, Kuermann J, Spormann AM, Gescher J. 2009. Periplasmic Electron Transfer via the c-Type Cytochromes MtrA and FccA of *Shewanella oneidensis* MR-1. Appl Environ Microbiol. 75(24): 7789-7796. 10.1128/AEM.01834-09

Tamao Y, Noguchi K, Sakai-Tomita Y, Hama H, Shimamoto T, Kanazawa H, Tsuda M, Tsuchiya T. 1991. Sequence Analysis of *nutA* Gene Encoding Membrane-Bound Cl~-Dependent 5'-Nucleotidase of *Vibrio parahaemolyticus.* J Biochem. 109, 24-29.

Venkateswaran K, Moser D, Dollhopf M, Lies D, Saffarini D, et al. 1999. Polyphasic taxonomy of the genus *Shewanella* and description of *Shewanella oneidensis* sp. nov. Int. J. Syst. Bacteriol. 49:705–24

Waterhouse A, Bertoni M, Bienert S, Studer G, Tauriello G, Gumienny R, Heer FT, de Beer TAP, Rempfer C, Bordoli L, Lepore, R, Schwede, T. 2018. SWISS-MODEL: homology modelling of protein structures and complexes. Nucleic Acids Res. 46(W1): W296-W303.

Webber G. 1950. Fluorescence of riboflavin and flavin-adenine dinucleotide. Biochem J. 47(1): 114–121.
Williams KP, Gillespie JJ, Sobral BW, Nordberg EK, Snyder EE, Shallom JM, Dickerman AW. 2010. Phylogeny of Gammaproteobacteria. J Bacteriol.192(9):2305-14. doi: 10.1128/JB.01480-09

Ziemke F, Hofle M, Lalucat J, Rossello-Mora R. 1998. Reclassification of *Shewanella putrefaciens* Owen's genomic group II as *Shewanella baltica* sp. nov. Int. J. Syst. Bacteriol. 48:179–86

Zou L, Huang Y, Long Z, Qiao Y. 2019. On-going applications of *Shewanella* species in microbial electrochemical system for bioenergy, bioremediation and biosensing. World Journal of Microbiology and Biotechnology. 35